






Cite this: *Analyst*, 2023, **148**, 5002

Elucidation of *N*-/*O*-glycosylation and site-specific mapping of sialic acid linkage isomers of SARS-CoV-2 human receptor angiotensin-converting enzyme 2†

Liming Wei, ^{‡a} Yuning Chen, ^{‡b,c} Xiaoxiao Feng,^a Jun Yao,^a Lei Zhang,^a Xinwen Zhou,^a Guoquan Yan,^a Hong Qiu,^{b,c} Chunhe Wang^{*b,c} and Haojie Lu  ^{*a}

Human angiotensin-converting enzyme 2 (hACE2) is the primary receptor for cellular entry of SARS-CoV-2 into human host cells. hACE2 is heavily glycosylated and glycans on the receptor may play a role in viral binding. Thus, comprehensive characterization of hACE2 glycosylation could aid our understanding of interactions between the receptor and SARS-CoV-2 spike (S) protein, as well as provide a basis for the development of therapeutic drugs targeting this crucial interaction. Herein, 138 *N*-glycan compositions were identified, most of which are complex-type *N*-glycans, from seven *N*-glycosites of hACE2. Among them, 67% contain at least one sialic acid residue. At the level of glycopeptides, the overall quantification of sialylated glycan isomers observed on the sites N322 and N546 have a higher degree of NeuAc (α 2–3)Gal (over 80.3%) than that of other *N*-glycosites (35.6–71.0%). In terms of *O*-glycans, 69 glycan compositions from 12 *O*-glycosites were identified, and especially, the C-terminus of hACE2 is heavily *O*-glycosylated. The terminal sialic acid linkage type of H1N1S1 and H1N1S2 are covered highly with α 2,3-sialic acid. These findings could aid the investigation of the interaction between SARS-CoV-2 and human host cells.

Received 28th June 2023,
Accepted 4th September 2023

DOI: 10.1039/d3an01079a

rsc.li/analyst

1. Introduction

Caused by severe acute respiratory syndrome coronavirus 2 (SARS-CoV-2), coronavirus disease-2019 (COVID-19) is a severe respiratory disease that has spread throughout the world since emerging near the end of 2019.¹ In the three and a half years since this virus emerged, seven SARS-CoV-2 mutants have evolved, each with high transmissibility and an increased risk for infection.^{2,3} To date, over 765.2 million people have been infected with SARS-CoV-2 and 6.9 million deaths due to COVID-19 have been recorded globally. Moreover, the epidemic has severely affected normal production and trade activities around the world, triggering a global economic recession.

Even though the WHO announced that the ongoing COVID-19 has not been a public health emergency of international concern recently, continued research is still needed to better understand SARS-CoV-2 infection to resist the possible occurrence of other mutants.

SARS-CoV-2 infects host cells *via* S protein, which interacts with hACE2 on the surface of host cells to initiate infection.^{4,5} hACE2 is a type I transmembrane protein expressed in human tissues such as lung, nasal, oral mucosa, heart, *etc.*^{6–9} Besides, the high expression of hACE2 is correlated with the high risk of SARS-CoV-2 infection.⁹ Notably, the function of favourable mutations in SARS-CoV-2 S protein exhibited higher binding affinity with hACE2.¹⁰ The key role of hACE2 may have contributed to multi-organ damage in COVID-19 patients to spark a pandemic by SARS-CoV-2 infection.¹¹ Hence, hACE2 is critical for both in-depth understanding of the infectious disease and the development of therapeutics. Both SARS-CoV-2 S protein and hACE2 are heavily glycosylated, which affects the interaction between SARS-CoV-2 S protein and hACE2.^{12–15} hACE2 has been reported to have high glycan occupancy (73.2 to 100%) at seven *N*-glycosylation sites, and one novel *O*-glycosylation site was deduced to be involved in viral binding.^{15,16} The glycans at N53, N90, and N322 on hACE2 are critical for SARS-CoV-2 S protein binding with hACE2.^{17,18}

^aInstitutes of Biomedical Sciences and Department of Chemistry, Fudan University, 131 Dongan Road, 20032 Shanghai, China. E-mail: luhaojie@fudan.edu.cn

^bShanghai Institute of Materia Medica, Chinese Academy of Sciences Department, 555 Zuchongzhi Road, 201203 Shanghai, China. E-mail: wangc@simmm.ac.cn

^cSchool of Pharmacy, University of Chinese Academy of Sciences, No. 19A Yuquan Road, 100049 Beijing, China

†Electronic supplementary information (ESI) available: Supplementary Table. See DOI: <https://doi.org/10.1039/d3an01079a>

‡These authors contributed equally to this work.



In this study, we combined ion mobility (IM)-mass spectrometry (MS) and high-resolution MS to characterize *N*- and *O*-glycosylation on hACE2 with the pretreatment of glycopeptides using ZIC-HILIC media. The mapping of α 2,3- or α 2,6-sialic acid linkage isomers on hACE2 was first reported at the glycopeptide level. Meanwhile, the complex *O*-glycan compositions of novel *O*-glycosites were determined. The linkage types of terminal sialic acid associated with the highly abundant *O*-glycans at the C-terminus of hACE2 were elucidated as well.

2.1. Chemicals and materials

Sequencing-grade modified trypsin and Glu-C protease were obtained from Promega (Madison, WI, USA). Proteinase K was purchased from Takara (Beijing, China). Peptide-*N*-glycosidase F (PNGase F) was obtained from New England Biolabs (Ipswich, MA, USA). Other chemical reagents were obtained from Sigma-Aldrich (St Louis, MO, USA). Analytical grade solvents and zwitterionic chromatography-hydrophilic interaction liquid chromatography (ZIC-HILIC) medium (5 μ m) were acquired from Merck (Darmstadt, Germany). A C18 solid-phase extraction cartridge was obtained from Waters Technology Co., Ltd (Shanghai, China).

2.2. Expression and purification of hACE2

The codon-optimized DNA fragment encoding extracellular hACE2 (residues 18–740) was sub-cloned into the mammalian expression vectors pTT5 (Addgene) with a 6× His-tag at the C-terminus. Purified plasmids were transfected into HEK293F cells and cultured in suspension with FreeStyle 293 expression medium (Gibco, CA, USA). After 6 days of culture, the cell culture medium was collected and purified by Ni-NTA chromatography. Protein purity was measured using SDS-PAGE gel (Bio-Rad Laboratories, Inc., CA, USA).

2.3. Sample preparation of hACE2 for glycosylation analysis

Purified hACE2 (200 µg in 25 mM NH₄HCO₃) was reduced and alkylated following the kit protocol (Applied Biosystems Inc., Foster City, CA). Subsequently, the protein was digested by incubating for 18 h at 37 °C first with trypsin and then with Glu-C.³² For *O*-glycosylation analysis of hACE2, N-linked glycans were removed from the denatured hACE2 sample by treating with PNGase F for 18 h at 37 °C. For the analysis of hACE2 C-terminal *O*-glycosylation, proteinase K was additionally applied at 37 °C overnight.

For the specific enrichment of *N*- or *O*-glycopeptides of hACE2, the resulting peptides were purified using a C18 solid-phase extraction column, freeze-dried, and enriched using the ZIC-HILIC tips as previously described.³³ The peptides were first dissolved in loading buffer consisting of 80% acetonitrile (ACN) and 1% trifluoroacetic acid (TFA) and then loaded onto a microtip containing 30 mg of ZIC-HILIC medium. After being washed with 200 μ L of loading buffer 6 times, the

The data from Synapt G2-Si were analyzed using the above parameters for the identification of *N*- and *O*-glycopeptides, except the mass tolerance for precursor and fragment ions was set as 20 ppm and 0.05 Da, respectively.

MassLyn 4.1 and DriftScope v2.9 (Waters) were applied for the data analysis performed using IM-MS. Arrival time distributions (ATDs) were extracted from raw data using MassLynx. Collision cross-section (CCS) values were estimated as described previously.³⁶ The area under the ATD of each isomer fragment was calculated using MassLyn 4.1 with the same spectral peak integral parameters and used for the mapping of α 2,3- and α 2,6-sialic acid linkage isomers on the specific glycopeptide.

Meanwhile, the eluted *N*- or *O*-glycopeptides from the chromatographic column were also fed into the ESI-MS system for detection using quadrupole time-of-flight ion-mobility mass spectrometry (IM-MS) (Synapt G2-Si, Waters, Milford, Massachusetts, USA). The parameters of mass spectrometry were set as follows: spray voltage, 2.2 kV; cone voltages, 30 V; source temperature, 100 °C; desolvation temperature, 250 °C. To further obtain the terminal sialic acid linkage isomers, targeted glycopeptides were isolated in the quadrupole and fragmented in the trap region before ion mobility separations. The parameters of IM-MS were set as follows: collision energy, 30 V; IMS cell pressure, ~2.66 mbar; N₂ gas flow, 90 mL min⁻¹; traveling wave height, 40 V; traveling wave velocity, 950 m s⁻¹; for CCS calibration, the MajorMix (Waters) in 0.1% FA was infused at 5 μL min⁻¹ with identical MS and IMS settings. Meanwhile, the signal intensity of precursor ions was limited at approximately 10⁵ counts per second to improve the accuracy of relative quantification of the sialic acid linkage isomer.³⁴ Three injection replications were carried out for all samples.

3. Results and discussion

3.1. N-Glycosylation of hACE2

Prior to analysis, the purity of the recombinant hACE2 was evaluated by SDS-PAGE (Bio-Rad Laboratories, Inc., CA, USA) (Fig. S1, ESI†). The single protein band shown in Fig. S1† proves the high purity of the recombinant hACE2. To allow for in-depth site-specific *N*/*O*-glycosylation and sialic acid linkage isomer analysis of hACE2, a series of enzyme digestion, specific enrichment, separation, and advanced fragmentation strategies were utilized in this study (Scheme S1†). By employing the step-energy collision dissociation mode using the Orbitrap Exploris™ 480, 1166 oxonium ion-containing tandem mass spectra were assigned to 406 unique glycopeptides, which consist of 128 *N*-glycans (Table S1a, ESI†). Based on the analysis of *N*-glycopeptides with Synapt G2-Si in the ramp-energy collision dissociation mode, 1661 oxonium ion-containing tandem mass spectra were assigned to 434 unique glycopeptides, in which 107 *N*-glycans were identified (Table S1b†). The overlap of the *N*-glycans identified by using two different mass spectrometers was about 63% at 1% FDR (Fig. S2†).

offer appropriate steric hindrance for the binding to SARS-CoV-2 S protein. In contrast, with their high heterogeneity and abundance, *N*-glycans on N90 may provide protection for host cells against viral infection, as also demonstrated by biophysical and mutation studies.^{7,41} The glycans on N90 and N103 in the above glycosylation elucidation of hACE2 are comparable in the great heterogeneity and distribution of each glycan type. It will benefit the synergic effect of glycans for the binding surface with the RBD of S protein.⁴¹ Meanwhile, the glycans on N546 may be involved in the interactions with the N74 and N165 glycans of S protein.¹⁵ The highly abundant glycosylation on N690 allows for glycan-protein interactions to maintain the hACE2 homodimer interface.³⁸ With the medium heterogeneity of glycans, N432 is distant from hACE2-RBD interaction sites. In summary, the *N*-glycosylation of hACE2 plays important roles in the stabilization of two hACE2 dimers and interaction with SARS-CoV-2 S protein. All of these binding sites should be further investigated for exploring the detailed molecular mechanism of host-virus interactions.

3.2. Mapping sialic acid linkage isomers of *N*-glycopeptides by IM-MS

As a common but complex post-translational modification, glycosylation on hACE2 has important implications for the SARS-CoV-2 S/hACE2 interaction.³⁷ In previous studies, N53 glycan on ACE2 was expected to have a dual and possibly competing role in heterodimer (ACE2-RBD) and homodimer (intra-ACE2) interactions.³⁸ Recently, N53 glycan has been proved to provide a positive contribution to hACE2-RBD binding and facilitate viral entry.¹⁸ It has also been shown that the glycans on N322 can strengthen S protein binding to hACE2.^{39,40} As a result of our findings, we hypothesize that fewer glycans on N53 may be advantageous in stabilizing the homodimer interface of hACE2 and interacting with the RBD heterodimer *via* glycan-glycan and glycan-protein binding. The low levels of glycosylation and heterogeneity on N322 may

Presented on different glycosites of hACE2, we found that the expression of α 2,3- and α 2,6-sialylation on the same glycan composition was also different. Taking the most dominant bi-antennary glycoform H5N4F1S1 for example, the glycopeptide IQ⁹⁰N_#LTVK modified with H5N4F1S1 showed $56.9 \pm 2.3\%$ α 2,3-sialylation (Fig. 3b), while the glycopeptide IS⁵⁴⁶N_#STEAGQK modified with H5N4F1S1 showed $78.0 \pm$

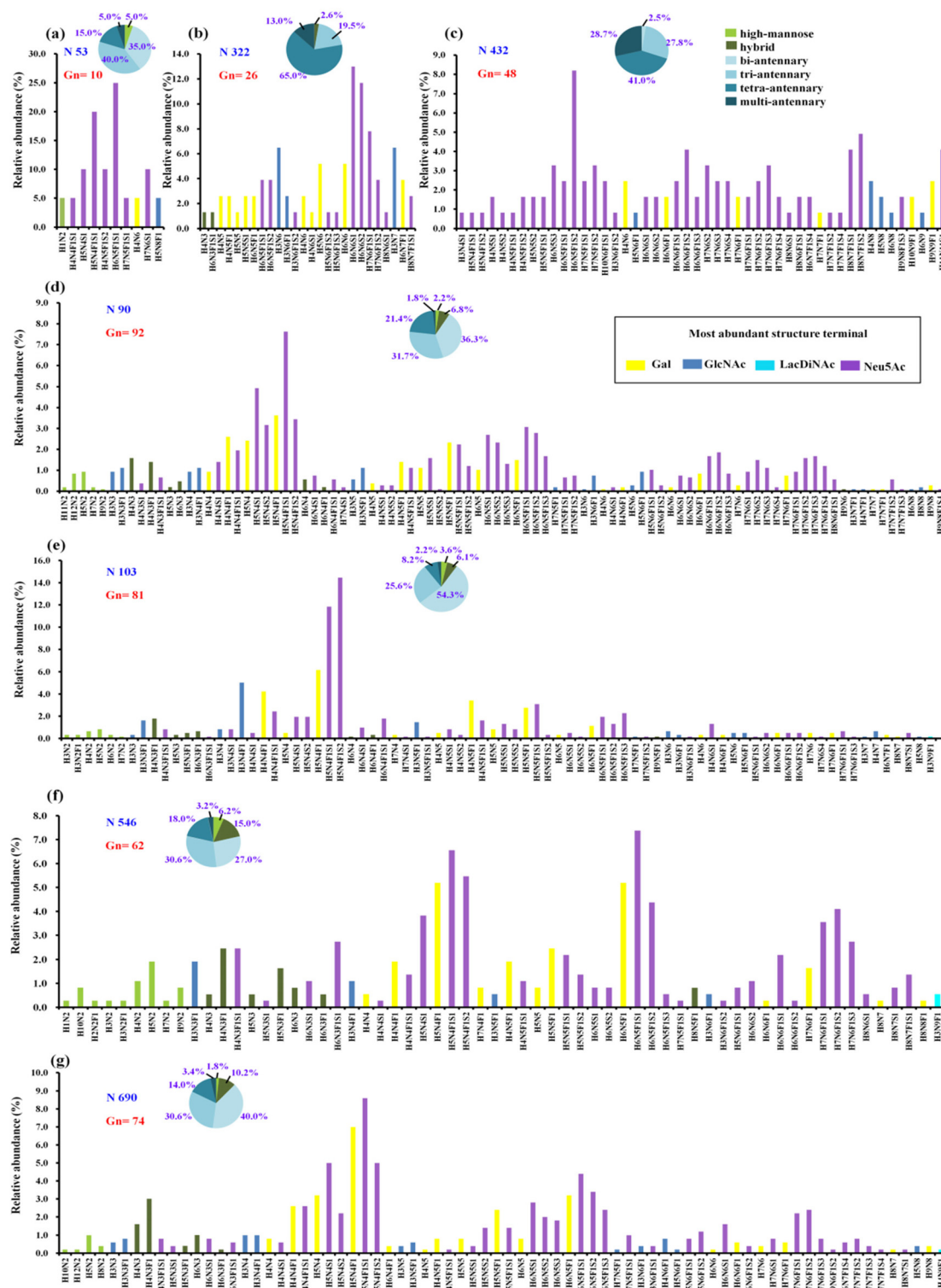


Fig. 1 The quantitative profiles of glycan composition on hACE2. (a–g) Glycopeptides of hACE2 were analysed with Scheme S1(a).† All seven sites of N-glycosylation are presented here. Displayed in the bar graphs are the individual compositions observed in term of relative abundances. According to the most abundant terminal glycan structures, the graphs are categorized and colored with different colors shown in legend. The pie charts summarize the relative quantification of these glycans simplified into different categories on specific N-glycosites (more details in Table S3†). (a) N53, (b) N322, (c) N432, (d) N90, (e) N103, (f) N546 and (g) N690. Gn represents the number of glycan composition assigned to the specific N-glycosites. N, HexNAc; H, Hex; F, fucose; S, sialic acid.



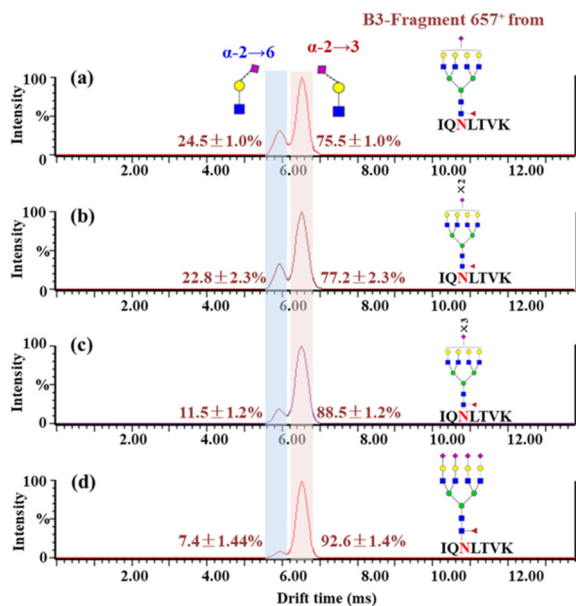


Fig. 2 Patterns of sialic acid linkage isomers of *N*-glycopeptides on hACE2. Glycosylated peptides 88–94 bearing a single *N*-glycosite (IQ⁹⁰N_#LTVK) were isolated and resolved by IM-MS. (a)–(d) Glycopeptide (IQ⁹⁰N_#LTVK) modified with glycan H7N6F1S1, H7N6F1S2, H7N6F1S3 and H7N6F1S4, respectively. The relative content of sialic acid isomers is indicated near each peak.

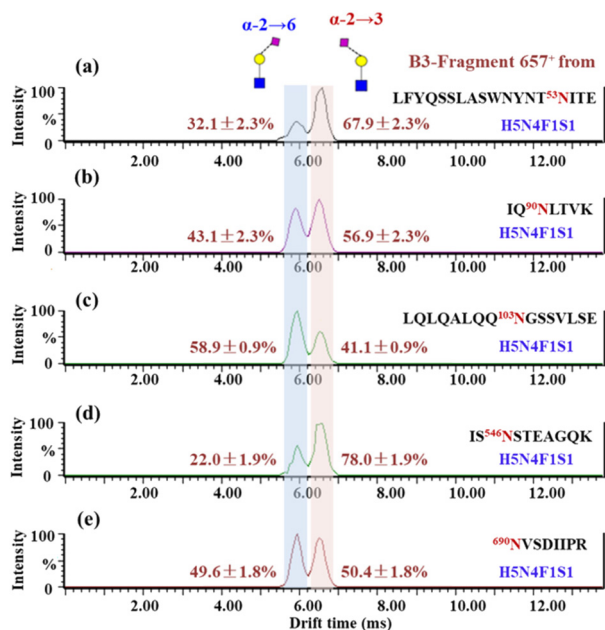


Fig. 3 ATDs of B3-trisaccharide fragments (*m/z* 657) from *N*-glycopeptides of hACE2 in panels a–e. (a) LFYQSSLASWNYNT⁵³NITE_{H5N4F1S1}, (b) IQ⁹⁰NLTVK_{H5N4F1S1}, (c) LQLQALQQ¹⁰³NGSSVLSE_{H5N4F1S1}, (d) IS⁵⁴⁶NSTEAGQK_{H5N4F1S1} and (e) ⁶⁹⁰NVSDIIPR_{H5N4F1S1}. The relative content of sialic acid isomers is indicated near each peak.

1.9% α2,3-sialylation (Fig. 3d). Meanwhile, the α2,3-sialylation content values in response to other sites modified with H5N4F1S1, *i.e.* N53, N103, and N690 were, respectively, 67.9 ±

2.3%, 41.1 ± 0.9%, and 50.4 ± 1.8% (Fig. 3a, c and e). This implies that H5N4F1S1 modification on hACE2 bears, on average, 58.9 ± 1.8% α2,3-sialylation. These phenomena are also observed on the different glycosites modified with tri-antennary glycan H6N5F1S1, on which the content of α2,3-sialylation ranges from 42.6 ± 1.2% to 94.8 ± 2.0% (Fig. S5†). In our analysis, the sialylation patterns showed different proportions not only on the different glycan compositions but also on the same glycan composition assigned to different *N*-glycosites of hACE2. Therefore, it is necessary to map the sialic acid linkage isomers of *N*-glycopeptides for the detailed characterization of hACE2. A total of 115 identified *N*-glycopeptides of hACE2 with glycans containing at least one sialic acid residue were selected for IM-MS analysis (CV < 10%, *n* = 3) (Table S4†). With a proportion of 91.3%, 105 out of 115 sialylated glycopeptides represented higher α2,3-sialylation. To determine the content of α2,3- and α2,6-sialylation on specific *N*-glycosites, the actual abundance of α2,3- and α2,6-sialylation was corrected by considering the relative abundance of glycopeptides. The pattern and distribution of α2,3- or α2,6-sialylation on *N*-glycopeptides and specific *N*-glycosites are summarized in Fig. 4 and Table S4†. In Fig. 4, N322 and N546 show a higher degree of α2,3-sialylation, bearing 80%, than the other five *N*-glycosites bearing 36–71%. Except for N53, which is predominant with 67% α2,6-sialylation, the sialylation patterns on other *N*-glycosites are dominated by α2,3-sialylation at the levels of both *N*-glycans and *N*-glycopeptides. The mapping of sialic acid linkage isomers on hACE2 was first summarized at the level of glycopeptides, when we observed relatively higher

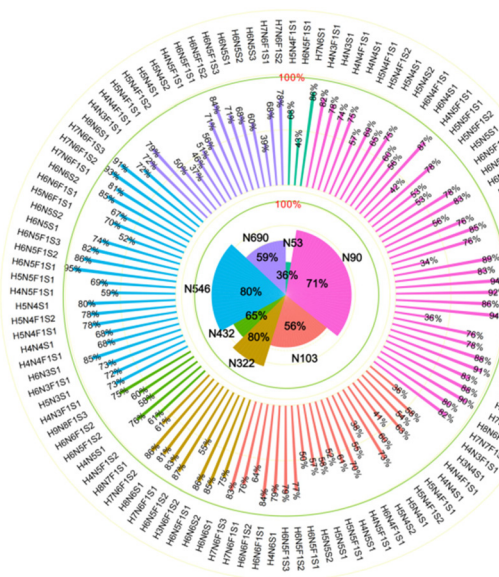


Fig. 4 The distribution of α2,3-sialylation on *N*-glycopeptides and specific glycosites of hACE2. The contents of α2,3-linked sialic acid isomer of glycans on specific *N*-glycosites are labeled in the outer circle, corresponding to the glycan compositions. The overall proportions of α2,3-sialylation presented on specific *N*-glycosites are illustrated in the inner circle. N53, N90, N103, N322, N432, N546 and N690 are colored green, pink, carmine, toast tan, grass green, blue, and purple, respectively.

3.3. O-Glycosylation of hACE2

In total, 69 *O*-glycan compositions, including 48 *O*-glycans attached to hACE2 were identified (Table S6†). Among the

To further assign the $\alpha 2,3$ - and $\alpha 2,6$ -sialylation of O-glycans at T730 and S740, the O-glycopeptides with high abundances of glycoforms were examined by IM-MS. The glycopeptide $\text{GIQP}^{730}\text{T}_{\#}\text{LGPP}$ bearing a single O-glycosite, modified with H1N1S1 and H1N1S2, and the glycopeptide $\text{GIQPTLGPNNQPPV}^{740}\text{S}_{\#}\text{GGGG}$ modified with H2N2S2, were analyzed by IM-MS (Fig. S23†). Following IM-MS analysis, the m/z 657 B_3 -type fragment from the above O-glycopeptides was assigned the sialylation of the corresponding O-glycans, as shown in Fig. 6. The extracted ATD of m/z 657 B_3 ions varies from distinct O-glycans. In Fig. 6a, the CCS of 235.4 \AA^2 of the only dominant peak from H1N1S1 at T730 is in agreement with the previously reported CCS of the $\alpha 2,3$ T-antigen sialylation.⁴⁴ With the monitored ATDs of m/z 657 B_3 ions from H1N1S2 at T730, two peaks were observed at 6.0 and 5.6 ms (Fig. 6b). The CCS of the first peak fits exactly the observed CCS of the $\alpha 2,3$ T-antigen sialylation, while the second peak with the CCS of 231.4 \AA^2 maps the CCS of $\alpha 2,6$ -sialylation on $\text{NeuAc}(\alpha 2-6)\text{GalGalNAc}$. The ratio of the $\alpha 2,3$ T-antigen sialylation to the $\text{NeuAc}(\alpha 2-6)\text{GalGalNAc}$ linkage is 1.2. There are three species with peaks at 6.0, 5.8 and 5.6 ms on S740 modified with H2N2S2 (Fig. 6c). The CCS of the first peak fits exactly that of $\alpha 2,6$ -sialylation on $\text{NeuAc}(\alpha 2-6)\text{GalGalNAc}$, while the CCS of the third peak fits with that of $\alpha 2,3$ T-antigen sialylation. To characterize the second peak, the standard glycopeptide ($\text{KVAN}_{\#}\text{KT}$) modified with H5N4S2, where the terminal NeuAc was connected to Gal through $\alpha 2-3$ and $\alpha 2-6$ bonds, was analyzed using IM-MS (Fig. S24†). We determined that the CCS of the m/z 657 B_3 ion fragment obtained by fragmentation of the standard glycopeptide with $\text{NeuAc}(\alpha 2-6)\text{GalGlcNAc}$ (CCS of 235.8 \AA^2) is in agreement with the second peak at 5.85 ms, which is a shoulder peak of the $\alpha 2,3$ T-antigen sialylation shown in Fig. 6c. Through five-pass cyclic IM-MS analysis, the fragment of $\text{NeuAc}(\alpha 2-6)\text{GalGlcNAc}$

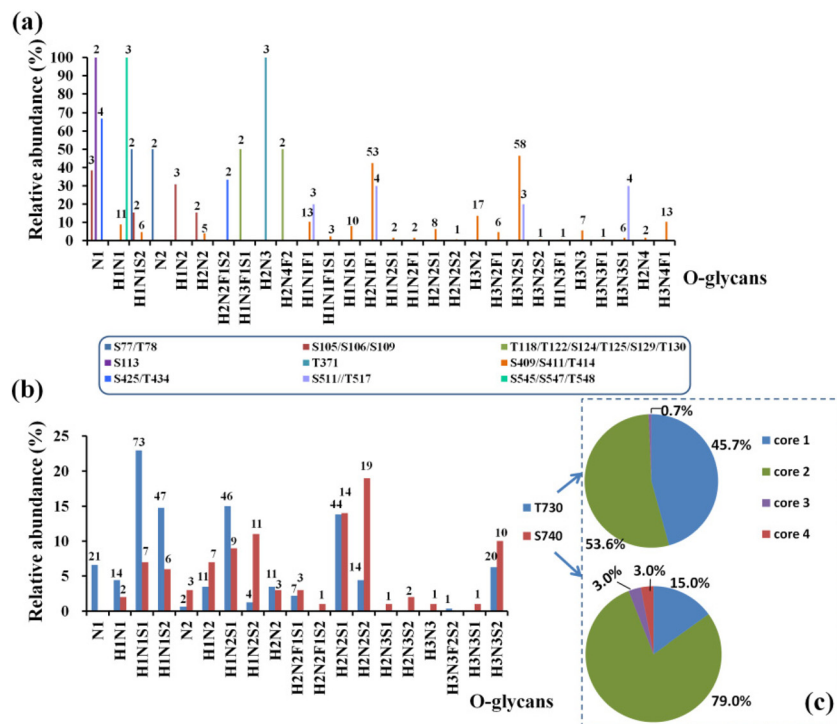


Fig. 5 The distribution and quantitative profile of *O*-glycans on hACE2, including the *O*-glycosites S77/T78, S105/S106/S109, S113, T118/T122/S124/T125/S129/T130, T371, S409/S411/T414, S425, S511/T517 and S545/S547/T548 (a), and T730 and S740 (b). (c) *O*-Glycan topologies were assigned to T730 and S740. The spectral counts for specific *O*-glycan are marked above the columns.

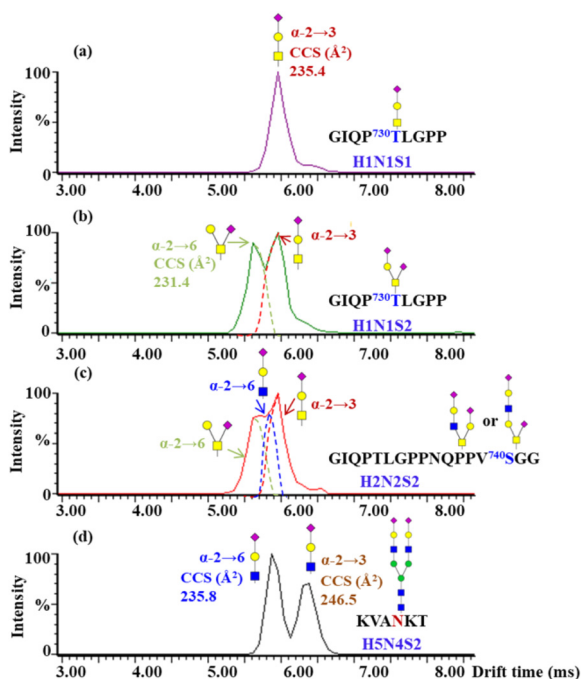


Fig. 6 ATDs of B3-trisaccharide fragments (m/z 657) from different *O*-glycopeptides of hACE2. The measured CCS assignments produced by the fragment of GIQPT⁷³⁰T_LLGPP modified with H1N1S1 (a), H1N1S2 (b), GIQPTLGPNNQPPV⁷⁴⁰S_#GGG modified with H2N2S2 (c) and standard *N*-glycopeptides with the peptide backbone of KVANK_#KT modified with H5N4S2 (d).

and α 2,3 T-antigen sialylation could attain obvious separation.⁴⁴ Lastly, T730 not only has high occupancy of *O*-glycans but is also highly capped with α 2,3-sialic acid of H1N1S1 and H1N1S2. In contrast to *N*-glycans, the *O*-glycan structures are more diverse, which greatly restricts the interpretation of glycan isomers. Thus, establishing the drift times of structures relevant to *O*-glycan in IM-MS will be essential for resolving different structures of *O*-glycans.

O-Glycans are associated with many critical biological functions, such as virus entry by binding onto its receptor, formation, and recognition by the cell immune system.^{45–48} Consistent with the *O*-glycomics, Zhao *et al.* reported that S155 and T730 at the C-terminus of hACE2 were *O*-glycosylated.¹⁵ Azadi *et al.* identified only one *O*-glycosite (T730) on hACE2 without pretreatment of *O*-glycopeptides.¹⁶ In our study, 12 *O*-glycosites were found in addition to the C-terminus of T730 and S740 using multi-enzymatic digestion and the HILIC enrichment method. However, the *O*-glycans present on hACE2 were of very low abundance at these identified *O*-glycosites, except for T730, S740, and S409/S411/T414. T730 and S740 are located in the collectrin-like domain close to the membrane. Adjacent to T730, L731 has been reported to be at the interface of ACE2 and B0AT1 (also called SLC6A19), which is a chaperone protein of ACE2. As an amino acid transporter, B0AT1 may block access of TMPRSS2s to the cutting site on ACE2. Further research indicates that the ACE2/B0AT1 dimer structure in the conformational binding of the SARS-CoV-2 S protein may

affect the viral invasion of host cells.⁴⁹ Thus, the heavily hydrophilic glycosylation at T730 and S740 may further affect the homodimer interaction and the ACE2/B0AT1 dimer structure on the cell surface. The simulation of RBD-bound and apo-ACE2 provides evidence that the flexibility in the ACE2 homodimer occurred not only at the linker connecting the transmembrane and head domains but also in the motions of the transmembrane helix in the membrane.³⁸ Whether the heavy *O*-glycosylation at the C-terminus of hACE2 is attributed to the flexibility in the conformational variability of hACE2 remains unclear. Moreover, adjacent to the transmembrane (TM) domain of hACE2, S740 and its modified *O*-glycans may interact with the lipid rafts on the cell. The cellular and molecular mechanisms of the interaction still need to be clarified. Here, we illustrated the possible sialic acid linkage isomer at the heavy *O*-glycans located on the C-terminus of hACE2, including H1N1S1, H1N1S2, and H2N2S2. α 2,3-Linked sialic acid is primarily capped on the terminus of H1N1S1 and H1N1S2, especially the core 1 structure, H1N1S1, on which only α 2,3-sialylation presented. Whether α 2,3-sialylation, presented on the *O*-glycans of hACE2, is involved in the infection and transmission of SARS-CoV-2 needs more in-depth and *in vivo* studies, which could aid the development of inhibitors to block the entry of SARS-CoV-2 into host cells.

4. Conclusions

In this study, we comprehensively determined site-specific *N*- and *O*-glycosylation patterns of hACE2 using complementary enzymatic digestion and specific enrichment methods combined with high-resolution MS. A total of 138 *N*-glycan compositions were determined for *N*-glycosites (N53, N90, N103, N322, N432, N546, and N690) and 91% were complex-type *N*-glycans. Meanwhile, N322 and N546 showed a higher degree of α 2,3-sialic acid linkage isomers of over 80.3% compared with the other *N*-glycosites (from 35.6 to 71.0%) using IM-MS analysis. For the first time, we identified 69 *O*-linked glycan compositions assigned to 12 *O*-glycosites, including T730 and S740 of hACE2. Furthermore, with high occupancy of *O*-glycans on T730, the terminal sialic acid linkage types of N1H1S1 and H1N1S2 were highly capped with α 2,3-sialylation. Our study substantially expands the glycoforms on hACE2 and provides a basis for further exploration of the function of glycosylation on hACE2, as well as its interactions with SARS-CoV-2 S protein.

Author contributions

All authors have accepted responsibility for the entire content of this manuscript and approved its submission. L. W., Y. C., H. Q., C. W. and H. L. designed the research; L. W., Y. C., X. F., J. Y., G. Y. and X. Z. performed the research; L. W., L. Z., H. Q.,

C. W. and H. L. analyzed data; and L. W., Y. C., X. F., J. Y., L. Z., G. Y., X. Z., H. Q., C. W., and H. L. wrote the paper.

Conflicts of interest

There are no conflicts to declare.

Acknowledgements

The work was supported by the Shanghai Science and Technology Program (22DZ2291700 and 22142202400), the National Key Research and Development Program of China (2016YFA0501303 and 2020YFE0202200), the NSF of China (Grant 21974025), the Shanghai Pujiang Program (18PJD002), the project supported by the Shanghai Municipal Science and Technology Major Project (Grant No. 2017SHZDZX01), and NHC Key Laboratory of Glycoconjugates Research (Fudan University). We would like to thank Ziqing Lin and Zachery R. Gregorich for critical reading of this manuscript. We thank Synapt G2-Si (Waters Co. UK) for providing the IM-MS analysis.

References

- 1 L. Wang and Y. Xiang, *Viruses*, 2020, **12**, 1289.
- 2 S. Kim, Y. Liu, Z. Lei, J. Dicker, Y. Cao, X. F. Zhang and W. Im, *J. Chem. Theory Comput.*, 2021, **17**, 7972–7979.
- 3 S. Pascarella, M. Ciccozzi, D. Zella, M. Bianchi, F. Benedetti, D. Benvenuto, F. Broccolo, R. Cauda, A. Caruso, S. Angeletti, M. Giovanetti and A. Cassone, *J. Med. Virol.*, 2021, **93**, 6551–6556.
- 4 A. C. Walls, Y. J. Park, M. A. Tortorici, A. Wall, A. T. McGuire and D. Veisler, *Cell*, 2020, **181**, 281–292.
- 5 G. Lu, Q. Wang and G. F. Gao, *Trends Microbiol.*, 2015, **23**, 468–478.
- 6 D. Wrapp, N. Wang, K. Corbett, J. A. Goldsmith, C. Hsieh, O. Abiona, B. S. Graham and J. S. McLellan, *Science*, 2020, **367**, 1260–1263.
- 7 W. Cao, C. Dong, S. Kim, D. Hou, W. Tai, L. Du, W. Im and X. F. Zhang, *Biophys. J.*, 2021, **120**, 1011–1019.
- 8 M. Y. Li, L. Li, Y. Zhang and X. S. Wang, *Int. J. Med. Parasit. Dis.*, 2020, **9**, 45.
- 9 H. Xu, L. Zhong, J. Deng, J. Peng, H. Dan, X. Zeng, T. Li and Q. Chen, *Int. J. Oral Sci.*, 2020, **12**, 8.
- 10 E. Socher, M. Conrad, L. Heger, F. Paulsen, H. Sticht, F. Zunke and P. Arnold, *J. Cell. Biochem.*, 2021, **122**, 1863–1872.
- 11 D. Santra, A. Banerjee, S. K. De, H. Thatoi and S. Maiti, *Comp. Clin. Pathol.*, 2023, **32**, 179–189.
- 12 J. Huang, D. Wang, R. D. Shipman, Z. Zhu, Y. Liu and L. Li, *Anal. Bioanal. Chem.*, 2021, **413**, 7295–7303.
- 13 D. Chang, J. A. Klein, M. R. Nalehua, W. E. Hackett and J. Zaia, *Anal. Bioanal. Chem.*, 2021, **413**, 7305–7318.



- 14 C. Huang, Z. Tan, K. Zhao, W. Zou, H. Wang, H. Gao, S. Sun, D. Bu, W. Chai and Y. Li, *iScience*, 2021, **24**, 103272.
- 15 P. Zhao, J. L. Praissman, O. C. Grant, Y. Cai, T. Xiao, K. E. Rosenbalm, K. Aoki, B. P. Kellman, R. Bridger, D. H. Barouch, M. A. Brindley, N. E. Lewis, M. Tiemeyer, B. Chen, R. J. Woods and L. Wells, *Cell Host Microbe*, 2020, **28**, 586–601.
- 16 A. Shajahan, S. Archer-Hartmann, N. T. Supekar, A. S. Gleinich, C. Heiss and P. Azadi, *Glycobiology*, 2020, 1–15.
- 17 J. D. Allen, Y. Watanabe, H. Chawla, M. L. Newby and M. Crispin, *J. Mol. Biol.*, 2021, **433**, 166762.
- 18 A. Isobe, Y. Arai, D. Kuroda, N. Okumura, T. Ono, S. Ushiba, S. I. Nakakita, T. Daidoji, Y. Suzuki, T. Nakaya, K. Matsumoto and Y. Watanabe, *Commun. Biol.*, 2022, **5**, 1188.
- 19 K. E. Shinya, M. Ebina, S. Yamada, M. Ono, N. Kasai and Y. Kawaoka, *Nature*, 2006, **440**, 435–436.
- 20 E. Qing, M. Hantak, S. Perlman and T. Gallagher, *mBio*, 2020, **11**, e02764.
- 21 M. A. Tortorici, A. C. Walls, Y. Lang, C. Wang, Z. Li, D. Koerhuis, G. J. Boons, B. J. Bosch, F. A. Rey, R. J. de Groot and D. Veisler, *Nat. Struct. Mol. Biol.*, 2019, **26**, 481–489.
- 22 M. Matrosovich, G. Herrler and H. D. Klenk, *Top. Curr. Chem.*, 2013, **367**, 1–28.
- 23 M. Cheng, H. Shu, M. Yang, G. Yan, L. Zhang, L. Wang, W. Wang and H. Lu, *Anal. Chem.*, 2022, **94**, 4666–4676.
- 24 M. Awasthi, S. Gulati, D. P. Sarkar, S. Tiwari, S. Kateriya, P. Ranjan and S. K. Verma, *Viruses*, 2020, **12**, 909.
- 25 A. N. Baker, S. J. Richards, C. S. Guy, T. R. Congdon, M. Hasan, A. J. Zwetsloot, A. Gallo, J. R. Lewandowski, P. J. Stansfeld, A. Straube, M. Walker, S. Chessa, G. Pergolizzi, S. Dedola, R. A. Field and M. I. Gibson, *ACS Cent. Sci.*, 2020, **6**, 2046–2052.
- 26 W. Li, R. J. G. Hulswit, I. Widjaja, V. S. Raj, R. McBride, W. Peng, W. Widagdo, M. A. Tortorici, B. Dieren, Y. Lang, J. W. M. Lent, J. C. Paulson, C. A. M. Haan, R. J. Groot, F. J. M. Kuppeveld, B. L. Haagmans and B. Bosch, *Proc. Natl. Acad. Sci. U. S. A.*, 2017, **114**, e8508–e8517.
- 27 Y. J. Park, A. C. Walls, Z. Wang, M. M. Sauer, W. Li, M. A. Tortorici, B. J. Bosch, F. DiMaio and D. Veisler, *Nat. Struct. Mol. Biol.*, 2019, **26**, 1151–1157.
- 28 L. Unione, M. J. Moure, M. P. Lenza, I. Oyenarte, J. Ereno-Orbea, A. Arda and J. Jimenez-Barbero, *Angew. Chem., Int. Ed.*, 2022, **61**, e202201432.
- 29 H. Chu, B. Hu, X. Huang, Y. Chai, D. Zhou, Y. Wang, H. Shuai, D. Yang, Y. Hou, X. Zhang, T. T. Yuen, J. P. Cai, A. J. Zhang, J. Zhou, S. Yuan, K. K. To, I. H. Chan, K. Y. Sit, D. C. Foo, I. Y. Wong, A. T. Ng, T. T. Cheung, S. Y. Law, W. K. Au, M. A. Brindley, Z. Chen, K. H. Kok, J. F. Chan and K. Y. Yuen, *Nat. Commun.*, 2021, **12**, 134.
- 30 Q. Yang, T. A. Hughes, A. Kelkar, X. Yu, K. Cheng, S. Park, W. C. Huang, J. F. Lovell and S. Neelamegham, *eLife*, 2020, **9**, e61552.
- 31 L. Nguyen, K. A. McCord, D. T. Bui, K. M. Bouwman, E. N. Kitova, M. Elaish, D. Kumawat, G. C. Daskhan, I. Tomris, L. Han, P. Chopra, T. J. Yang, S. D. Willows, A. L. Mason, L. K. Mahal, T. L. Lowary, L. J. West, S. D. Hsu, T. Hobman, S. M. Tompkins, G. J. Boons, R. P. de Vries, M. S. Macauley and J. S. Klassen, *Nat. Chem. Biol.*, 2022, **18**, 81–90.
- 32 H. Li, Y. Wang, L. Zhang, H. Lu, Z. Zhou, L. Wei and P. Yang, *Analyst*, 2015, **140**, 7886–7895.
- 33 P. Fang, J. Xie, S. Sang, L. Zhang, M. Liu, L. Yang, Y. Xu, G. Yan, J. Yao, X. Gao, W. Qian, Z. Wang, Y. Zhang, P. Yang and H. Shen, *Anal. Chem.*, 2020, **92**, 867–874.
- 34 X. Feng, H. Shu, S. Zhang, Y. Peng, L. Zhang, X. Cao, L. Wei and H. Lu, *Anal. Chem.*, 2021, **93**, 15617–15625.
- 35 Y. Zhang, W. Zhao, Y. Mao, Y. Chen, J. Zhu, L. Hu, M. Gong, J. Cheng and H. Yang, *Front. Chem.*, 2021, **9**, 689521.
- 36 M. Guttman and K. K. Lee, *Anal. Chem.*, 2016, **88**, 5212–5217.
- 37 J. Huang, S. Hou, J. An and C. Zhou, *Anal. Bioanal. Chem.*, 2023, **415**, 1455–1464.
- 38 E. P. Barros, L. Casalino, Z. Gaieb, A. C. Dommer, Y. Wang, L. Fallon, L. Raguette, K. Belfon, C. Simmerling and R. E. Amaro, *Biophys. J.*, 2021, **120**, 1072–1084.
- 39 W. Li, C. Zhang, J. Sui, J. H. Kuhn, M. Moore, S. Luo, S. Wong, I. Huang, K. Xu, Y. He, W. A. Marasco, Y. Guan, H. Choe and M. Farzan, *EMBO J.*, 2005, **24**, 1634–1643.
- 40 A. R. Mehdipour and G. Hummer, *Proc. Natl. Acad. Sci. U. S. A.*, 2021, **118**, e2100425118.
- 41 B. Wang, J. Zhao, S. Liu, J. Feng, Y. Luo, X. He, Y. Wang, F. Ge, J. Wang, B. Ye, W. Huang, X. Bo, Y. Wang and J. J. Xi, *Emerging Microbes Infect.*, 2022, **11**, 1488–1499.
- 42 T. Nishikaze, H. Tsumoto, S. Sekiya, S. Iwamoto, Y. Miura and K. Tanaka, *Anal. Chem.*, 2017, **89**, 2353–2360.
- 43 W. Tian, D. Li, N. Zhang, G. Bai, K. Yuan, H. Xiao, F. Gao, Y. Chen, C. C. L. Wong and G. F. Gao, *Cell Res.*, 2021, **31**, 1123–1125.
- 44 M. Sanda, L. Morrison and R. Goldman, *Anal. Chem.*, 2021, **93**, 2003–2009.
- 45 I. Bagdonaite, R. Norden, H. J. Joshi, S. L. King, S. Y. Vakhrushev, S. Olofsson and H. H. Wandall, *J. Biol. Chem.*, 2016, **291**, 12014–12028.
- 46 E. J. Simon and A. D. Linstedt, *J. Biol. Chem.*, 2018, **293**, 19866–19873.
- 47 D. S. Roberts, M. Mann, B. H. Li, D. Kim, A. R. Braiser, S. Jin and Y. Ge, *Chem. Sci.*, 2022, **13**, 10944–10949.
- 48 D. S. Roberts, M. Mann, J. A. Melby, E. J. Larson, Y. Zhu, A. R. Brasier, S. Jin and Y. Ge, *J. Am. Chem. Soc.*, 2021, **143**, 12014–12024.
- 49 R. Yan, Y. Zhang, Y. Li, L. Xia, Y. Guo and Q. Zhou, *Science*, 2020, **367**, 1444–1448.

